Chain Conformation in Ultrathin Polymer Films Using Small-Angle Neutron Scattering

Ronald L. Jones and Sanat K. Kumar*

Department of Materials Science and Engineering, Pennsylvania State University, University Park, Pennsylvania

Derek L. Ho and Robert M. Briber

Department of Materials and Nuclear Engineering, University of Maryland, College Park, Maryland

Thomas P. Russell

Polymer Science and Engineering Department, University of Massachusetts, Amherst, Massachusetts

Received June 29, 2000; Revised Manuscript Received October 16, 2000

ABSTRACT: Small-angle neutron scattering (SANS) experiments were conducted on isotopic polystyrene blend films spin-coated onto hydrogen passivated silicon wafers over a wide range of wavevectors, q ($0.56 \leq qR_{G,bulk} \leq 50$, where $R_{G,bulk}$ is the unperturbed radius of gyration of the chains). The films thickness varied from "bulk" ($D/R_{G,bulk} \approx 50$, where D is the film thickness) to smaller than $R_{G,bulk}$ ($\approx$10 nm, i.e., $D/R_{G,bulk} \approx 0.5$). Samples were annealed for long times at temperatures well above the glass transition temperature to ensure thermal equilibrium and then quenched to room temperature. Scattering experiments were then performed in a transmission geomtery. Analysis of the data using the RPA model (most appropriate for $qR_{G,bulk} \leq 1$) and the Kratky approach ($4 \leq qR_{G,bulk} \leq 50$) independently confirms that the chains retain their unperturbed Gaussian conformations in the direction parallel to the surfaces, i.e., normal to the confinement direction. These results lend significant credence to computer simulations and past analytical theories, which suggest that chain conformation in these thin films can be viewed as reflected random walks.

1. Introduction

The modification of macromolecular chain conformations in confined environments underpins any changes in the properties of thin films from their bulk values, e.g., the glass transition, permeability, and miscibility. Monte Carlo and molecular dynamics simulations[1−5] have shown that chain dimensions in a direction normal to the surfaces (i.e., along the confinement direction) are significantly modified when the film thickness D becomes smaller than $4R_{G,bulk}$. In contrast, chain dimensions and conformations parallel to surfaces are unaltered (i.e., perturbed less than 10%) even when $D \approx R_{G,bulk}$. These results are in agreement with an early conjecture of Silverberg,[6] who assumed that chain conformations in thin melt films could be modeled by Gaussian chains reflected at the interfaces ("reflected Gaussian approximation").

Available experimental data on thin films, e.g., birefringence,[7] chain orientation,[8] self-diffusion coefficients,[9] and thermal expansivity, and, hence, the glass transition,[10−14] consistently deviate from their bulk values for film thicknesses smaller than ≈4−10 times $R_{G,bulk}$. Similarly, it was found that poly(ethylenepropylene), which normally wets silicon, could be made to dewet this substrate if film thicknesses were reduced below $4R_{G,bulk}$.[15] The modification of properties for these film thicknesses has led to speculations that chain conformations should also be perturbed in these situations.

Attempts to measure chain conformations in thin polymer films have been limited by the small volume of the sample. Porous media have been used to circumvent this problem, but the random orientation of the pores in typical porous media makes data interpretation ambiguous.[16−21] Shuto and co-workers attempted to overcome this problem by stacking multiple films on a single planar substrate by a Langmuir−Blodgett film deposition technique.[22,23] These films could not be annealed since this would permit the interdiffusion of polymers in the different layers, thus destroying the thin film geometry obtained in the as-cast state. Using small-angle neutron and X-ray scattering of these monolayers, the radius of gyration was found to increase significantly (≈50%) in films where $D < 2R_{G,bulk}$. Similar results were also found by Stamm and co-workers on isotopic mixtures of polystyrene,[24] where grazing incidence neutron scattering was employed. These films were not annealed to ensure that the concentration profiles of both species were uniform in the film. Later studies,[25] using transmission electron microscopy of block copolymers, revealed that the method of casting could produce nonequilibrium stretching of the chains. Consequently, these past results, which were obtained from as-cast films, may be influenced by the nonequilibrium nature of the film formation process.

Recently, Brulet et al.[26] performed SANS on spin-cast and subsequently annealed isotopic polystyrene blend films. Operating exclusively in the Kratky regime ($R_{G,bulk}/l_p \gg qR_{G,bulk} \gg 1$, where l_p is the persistence length), these workers examined local changes in chain conformations in thin films. A substantial increase in l_p, from its bulk value of ≈0.9 nm to 4.5 nm, in films of $D = 10$ nm, was found. These results are in contradiction with most simulations and our previous SANS

10.1021/ma001141o CCC: $20.00
Published on Web 01/06/2001

Table 1. Molecular Weights and Distributions for Polystyrenes Used in This Work

dPS	289 000	1.04	hPS	284 000	1.05
dPS	674 000	1.08	hPS	697 000	1.05

results where, using a similar geometry, the chain dimensions parallel to the surface were found to be unaffected by confinement.[27] Our previous experiments were performed under conditions where $qR_{G,bulk} \approx 1$, and therefore our data did not overlap signficantly with the experiments of Brulet et al. Consequently, a systematic and critical comparison of the two experimental protocols could not be performed. Here we report studies over a much broader q range, encompassing both the Zimm and Kratky regimes, allowing a comprehensive elucidation of chain conformation in thin films.

Recent improvements in flux at the cold neutron source at the National Institute of Standards and Technology (NIST) have permitted the extension of a standard bulk characterization technique, small-angle neutron scattering (SANS), to ultrathin polymer blend films.[27−29] Two factors strongly limited this extension. First, the volume of material decreases with decreasing thickness, and for $D < 100$ nm, statistically significant data could not be obtained in reasonable time scales. Several wafers with identically prepared films (up to 20) are stacked in series in the beam path to alleviate this problem. Second, with decreasing film thickness the contribution of surface roughness to the total scattering increases, especially at low q. This roughness contribution must be properly accounted for in data analysis.

Here we present scattering data from thin films (10 nm $\leq D \leq 1$ μm) over a broad wavevector range ($0.04 \leq q \leq 2.0$ nm^{-1}) from two separate isotopic polystyrene blends. We shall conclusively show that the scattering data from both the low-q regime and the Kratky regime are independently consistent with an invariance of chain dimensions normal to the confinement direction as a function of film thickness. Thus, chain dimensions parallel to the surfaces are equal to their unperturbed bulk values down to $D/R_{G,bulk} \approx 0.5$. These results are in good agreement with simulations and theoretical arguments. The broader impact of these results, especially on the dynamic properties of thin polymer films, are discussed.

2. Experimental Section

Perdeuterated and normal polystyrenes, dPS and hPS, respectively, with narrow molecular weight distributions ($M_w/M_n \leq 1.08$) were purchased from Polymer Source (Table 1). Two isotopic polystyrene mixtures of 25 wt % dPS/75 wt % hPS, with matched molecular weights of ≈270 000 ($M_w/M_n <$ 1.05) and ≈650 000 ($M_w/M_n < 1.08$) respectively (Table 1), were studied. These chains have $R_{G,bulk} \approx 14$ and 22 nm, respectively. These systems are expected to have upper critical solution type phase behavior with bulk spinodal temperatures estimated to be ≈−118 °C for the 270K mixture and ≈12 °C for the 650K blend.[30] Films of varying thickness in the range 1 μm down to 10 nm were spin-coated onto silicon wafers at 1500−3000 rpm from 0.5 to 3 wt % toluene solutions. The Si wafers were cleaned with a heated piranha etch (30/70 by weight H_2O_2/H_2SO_4) and then an HF etch (to remove the native oxide layer). PS wets the resulting hydrogen passivated surfaces. Single wavelength ellipsometry and X-ray reflectivity were used to determine film thickness. The samples were annealed at 120° C for times ranging from 8 to 100 h and quenched to room temperature into the glassy state ($T_g \approx 105$ °C). Under these conditions the bulk blends are well mixed and far from the phase boundary.

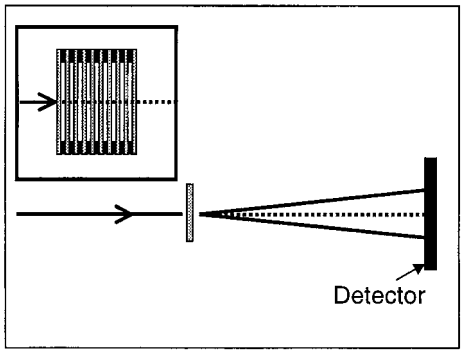

Figure 1. Schematic of SANS sample geometry. Depicted is the thin film relative to incident (solid line with arrow), scattered (solid line), and transmitted (dotted line) neutron beams. The sample stack, indicated as the gray block and detailed in the inset, features films perpendicular to the incident beam. The scattering vector is primarily in the xy plane, normal to the film.

Up to 20 identically prepared films on separate silicon substrates were stacked in series in the neutron beam to enhance the signal-to-noise (see Figure 1). Silicon wafers with (100) and (111) crystal orientations were employed. The extremely low probability of a scattering event ($P_{scatter} \approx 8 \times 10^{-4}$ in a film of thickness 1 μm) suggests that multiple scattering is unimportant. By measuring stacks of varying numbers of films, we established that this procedure did not introduce artifacts into the results reported. Since the transmission of a stack of 20 bare wafers was virtually identical to that of the empty sample holder, we utilized the empty beam as the background in the correction of the scattering data. The raw data were corrected for background noise, empty cell, and detector efficiency, circularly averaged, and then placed on an absolute intensity scale relative to a silica standard. In this context it must be stressed that any incoherent scattering has *not* been subtracted at this stage, and this correction will be discussed below in the context of the experimental results. For all films studied, analogous bulk samples of the same molecular weight and composition were cast from solution, as reported previously.[27] Standard errors in scattered intensity were calculated as described previously.[29] In addition to the error analyses of the RPA, errors in segment length were also calculated using the best fit to the Kratky equation. Since these two methods provided comparable errors, we only report the Kratky results here. Using a procedure outlined elsewhere,[30] the error in χ was calculated.

The SANS measurements were performed at the NIST Center for Neutron Research (NCNR) at the National Institutes of Standards and Technology (NIST) in Gaithersburg, MD. In the small angle geometry sketched in Figure 1, the scattering vector is primarily in the plane of the films, and hence our measurements are primarily sensitive to chain conformations in this direction. Data were collected over a 2 year span on the NG3 (30 m SANS), NG7 (30 m SANS), and NG1 (8 m SANS) beam lines. For Si(111) substrates we utilized a wavelength $\lambda \geq 0.8$ nm to preclude Bragg diffraction effects. Since the beam intensity at $\lambda = 0.8$ nm is significantly smaller than the peak at $\lambda = 0.5$ nm, Si(100) substrates were exclusively used for measurements in the Kratky regime at higher q. In these cases, higher intensity $\lambda = 0.6$ nm neutrons were employed. The two different 30 m instruments had slightly different wavelength resolution ($0.11 < \delta\lambda/\lambda < 0.22$). The effects of this variation on the data were within experimental uncertainties in the case of bulk samples. With the exception of the 8 m SANS experiments, collimation was set with a presample flight path of 10.0 m (four waveguides), a sample−detector distance of 10.8 m, and a sample aperture of 0.0191 m. The 8 m SANS configuration had a fixed flight path of 8.0 m and a sample aperture of 0.0191 m.

3. Chain Conformation

3.1. Kratky Regime. Recent experiments by Brulet et al.[26] suggested that chain persistence lengths increase dramatically with decreasing thickness in the case of polystyrene films with $D \leq 100$ nm. These experiments focused on the Kratky regime at higher q ($0.3 < q < 1.0$ nm^{-1}), where $q^2I(q)$ is effectively independent of the thermodynamics of the system and, thus, only yields information on the conformations of chains. In the case of Gaussian chains the plateau value of $q^2I(q)$ is

$$q^2I(q) = \frac{12k_N v_0 \phi(1-\phi)}{\sigma^2} \quad (1)$$

k_N is the neutron contrast factor, σ is the statistical segment length of the chains, and v_0 is the reference volume. Similar results can also be derived for wormlike chains,

$$q^2I(q) = \frac{6k_N v_0 \phi(1-\phi)}{a l_p} \quad (2)$$

where a is the monomer step length. Note that the asymptotic value of $q^2I(q)$ decreases with increasing l_p. For even larger q values, where $ql_p > 1$, the plot of $q^2I(q)$ will be dependent on q. The crossover from a q-independent value to a q-dependent value for $q^2I(q)$ gives another measure of the persistence length of the chains.

Brulet et al.[26] examined two matched isotopic polystyrene blends, whose molecular weights were very similar to those in Table 1. The films were spin-coated on *unetched* Si wafers. Two film thicknesses (10 and 100 nm, respectively) were examined before and after annealing. Their data indicate dramatic changes in the molecular size upon confinement; i.e., l_p values of 4.5 nm were observed for annealed films of $D = 10$ nm. However, the modeling of the experimental data by a wormlike chain model is questionable since the plateau value of $q^2I(q)$ increases with decreasing film thickness, while it might have been expected to decrease following eq 2.

Prior studies by our group were limited to a lower q range ($q < 0.3$ nm^{-1}). Here we expand these studies to a much broader range ($0.04 < q < 2.0$ nm^{-1}), even broader than that employed by Brulet et al.[26] Figure 2 shows data obtained from a 650K blend of thickness 33 nm and a corresponding bulk sample, corrected for all factors except the incoherent background. This Kratky plot illustrates that $q^2I(q)$ increases with q as reported by Brulet et al.[26] even for the bulk samples. Comparison of our data to those of Brulet, however, shows that the magnitude of the increase in our data is not as large, even though the wavevector range accessed in our experiments is roughly twice as large as in ref 26.

To quantify the contribution of incoherent scattering, we have conducted three different experiments. First, we measured the scattering from a bulk hPS sample. A plot of $I(q)$ vs q in Figure 3 shows that the scattering in this case is independent of q and assumes a reasonable value of $\approx$0.5 cm^{-1}. Bulk dPS samples essentially do not scatter at large q when examined on this basis ($I_{\text{incoh,dPS}} \approx 0.06$ cm^{-1}). On the basis of an overall composition of 75 wt % hPS, therefore, a total incoherent background ($=\phi I_{\text{dPS}} + (1-\phi)I_{\text{hPS}}$) of 0.38 cm^{-1} needs to be subtracted. An alternative means of obtaining the background relevant to the thin film experiments is as follows: six wafers were coated with PSH films of thickness 140 nm, and two were coated with PSD films of thickness 180 nm. This stack was then run in a standard SANS mode after annealing for 8 h. The scattering from this stack is q-dependent and appears to plateau at a value of 1 cm^{-1} at high q (Figure 3). Consequently, this sample shows more than incoherent scattering. To clarify why the stacks scatter significantly more than the bulk hPS sample, especially at high q, we have run stacks of bare Si wafers but found virtually no scattered intensity above the empty, or sample free, beam. Similarly, since stacks of pure hPS scattered significantly less than the bulk dPS, we conclude that roughness at the air and the substrate interfaces of the dPS films are responsible for the excess scattering (discussed below). The low intensity at high q prevents an accurate determination of the q-independent background in the thinnest films. As q increases, the intensity decreases, and therefore the background of the pure dPS-hPS stack at $q = 2.0$ nm^{-1} is expected to be lower than that observed in Figure 3, where $q_{\max} = 1.0$ nm^{-1}. However, as D decreases, the overall intensity increases dramatically. Consequently, the background of 1 cm^{-1} should be viewed only as an approximate estimate of the background of a much thinner film.

Figure 4 is a plot of data from the thin film data set shown in Figure 2, with a subtraction of 0.38 and 1.0 cm^{-1} from the intensity data. The bulk sample was analyzed with a 0.38 cm^{-1} background. The data from

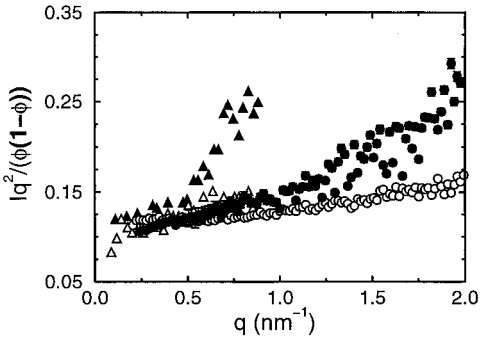

Figure 2. Kratky plot of 650K hPS/dPS thin film blends. Plotted are data from a film of thickness 33 nm (filled circles) and the analogous bulk (open circles). In addition, data scanned from ref 26 for a 660K blend are plotted for thicknesses of 100 nm (open triangles) and 10 nm (filled triangles). The y-axis is scaled by the factor $\phi(1-\phi)$ to account for differences in composition between the experiments of Brulet et al. ($\phi = 50$ wt % dPS) and this work ($\phi = 25$ wt % dPS). In all cases, data have been analyzed without subtraction of incoherent scattering of the pure components.

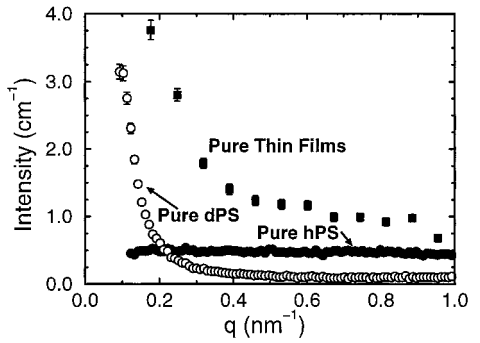

Figure 3. Intensity per unit volume vs q for pure hPS (filled circles), pure dPS bulks (open circles), and an eight-wafer stack comprised of six pure hPS films and two dPS films (filled squares).

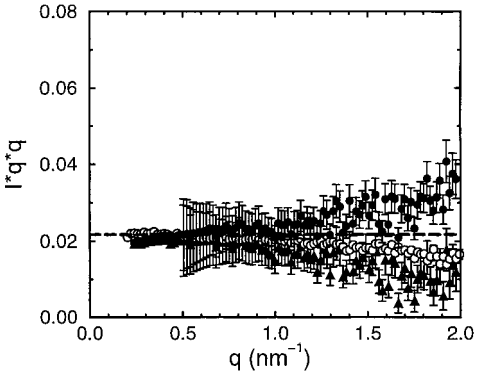

Figure 4. Kratky plot of 650K hPS/dPS thin film blends; samples are the same as in Figure 2. A constant factor of 1.0 (filled triangles) and 0.38 cm^{-1} (filled circles) has been subtracted from the 33 nm film, and 0.38 cm^{-1} is subtracted from bulk (open circles) to account for incoherent scattering. Dashed line is solution of eq 1 using $\sigma = 0.68$ nm.

all three analyses suggest that $q^2I(q)$ effectively assumes a wavevector-independent value up to the highest q value examined. Further, since the plateau obtained from both thin film analyses are virtually identical to that obtained from a bulk sample, we are left with the simple result that the statistical segment length of chains in films as thin as $D/R_{G,bulk} \approx 0.5$ are indistinguishable from the bulk, i.e., $\sigma = 0.68$ nm (dashed line in Figure 4). As mentioned previously, the thin film background of 1 cm^{-1} is only an approximate estimate. Its lower bound is 0.38 cm^{-1}, and backgrounds higher than 1 cm^{-1} would result in an even more pronounced downward curvature to Iq^2. In no case do we see evidence of an upward curvature of Iq^2 comparable to those reported by Brulet et al.[26] Possible sources for the inconsistency between our measurements and those of Brulet et al. are the following:

(i) The samples of Brulet et al. were cast on unetched Si wafers. PS will dewet the native oxide layer of silicon, with this propensity increasing with decreasing thickness.[31] While no overt signs of deweting were observed in Brulet's experiments, it is important to note that the Kratky plateau of their as-cast 100 nm films are very similar to those anticipated from bulk data (see Figure 1 of ref 26). It is only on annealing that a large increase of $q^2I(q)$ is reported at high q.

(ii) Brulet et al. do not subtract the background resulting from the protonated polymer or the roughness contribution from the dPS films. As we have shown above, this background can be substantial even in the case of the bulk samples (see Figure 2) and plays an increasingly significant role in determining the high-q behavior with decreasing thickness.

The data presented here, acquired over a very broad q range, strongly suggest that chains retain their unperturbed Gaussian conformations in the direction parallel to the surfaces as deduced by a Kratky analysis. While there are some questions concerning background subtraction, these results will be substantiated by a detailed analysis of low-q data in the Guinier regime. We finally note that our results are in stark contrast to the work of Brulet et al. and are in excellent agreement with results obtained from computer simulations for polymer melts in confined geometries.

3.2. Guinier Regime. An important contribution to the low-q scattering arises from roughness at the air and substrate interfaces. This contribution, which becomes more prominent for thin films of the low molecular weight blends, must be properly separated from the scattering arising from concentration fluctuations in the system.

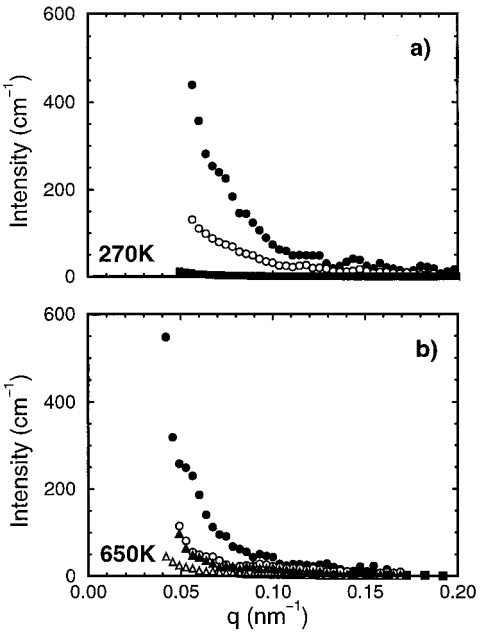

Figure 5. Intensity vs q plot for pure dPS films. Shown are results from films of molecular weight (a) 270K and (b) 650K from films of thickness (270K) 17 nm (solid circles), 60 nm (open circles), and bulk (solid triangles); (650K): 15 nm (solid circles), 37 nm (open circles), 46 nm (closed triangles), 315 nm (open triangles), and bulk (solid squares).

3.2.1. Interfacial Scattering. Scattering from bulk dPS should only arise from thermal fluctuations. This scattering should be weak and angularly independent. However, the bulk dPS in Figure 3 shows excess, q-dependent scattering that must arise from either the incomplete deuteration (≈99%) of the PS or voids. Partial deuteration can be eliminated as the primary cause of this scattering by using arguments of Balsara et al.[32] Therefore, voids or impurities within the polymer give rise to the excess scattering. In addition, as shown in Figure 5, the scattering intensity at low q increases dramatically with decreasing thickness for both molecular weights. The data are analyzed per unit volume, which assumes that all the scatterers in the sample contribute equally to the measured intensity. Plots of the thin film data on a per area basis ($I(q)D$, where D is the film thickness) are independent of D, especially for $D \leq 315$ nm (see Figure 6). This suggests that the scatttering from the thinnest dPS films arises from the interfaces of the film and not from the bulk of the sample.

The importance of surface roughness in SANS experiments on thin films has been emphasized in previous work[29] where it was found that substrate roughness of rms amplitude of 3 nm with lateral features ≈1 μm in size could yield anomalous low-q scattering. Not explicitly separating this component from the concentration fluctuation contribution could lead to erroneous conclusions. For example, uncorrected data would have led us to conclude that a 15 nm, 270K dPS/hPS blend is phase-separated at 120 °C.[29]

X-ray reflectivity shows that films (15 nm $\leq D \leq$ 100 nm) have an rms roughness of 0.5−1.0 nm, at both the silicon and the air interfaces. The scattering contrast, k_N, for dPS/vacuum ($k_N = 6.76 \times 10^5$ mol/m^4) is more

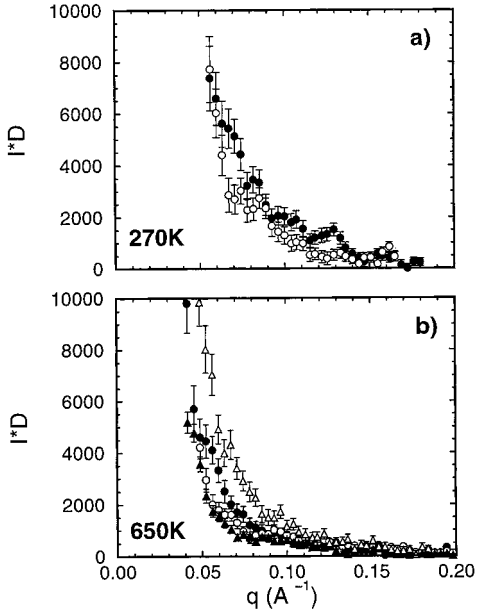

Figure 6. Intensity per unit area (*ID*) vs *q* plot for pure dPS films. Symbols are identical to those in Figure 5.

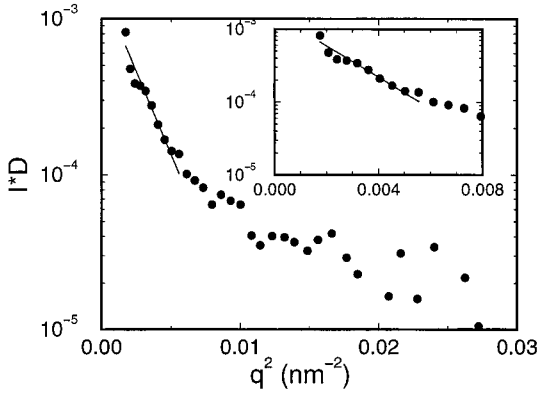

Figure 7. Intensity vs q^2 for 15 nm, 650K pure dPS films (solid circles). The line indicates a fit to the lowest *q*-vector points using the capillary wave analysis provided in the text. The fit range is shown in more detail in the inset.

than twice that of the dPS/Si ($k_N = 3.07 \times 10^5$ mol/m^4). If both interfaces were equally rough, the scattering from the dPS/air interface will dominate surface scattering. The form factors for roughness arising from capillary waves at liquid surfaces are well-known in a reflection geometry. This analysis was extended to the transmission geometry of SANS. Sinha reports a generalized form factor for capillary waves in which the relevant cutoff is the coherence length of the neutron beam, ζ ($\approx$1 μm in our experiments).[33] Applying this form in the limit of $q_z \rightarrow 0$, where q_z is the component of the wavevector normal to the substrate, after subtraction of the specular component, yields

$$S(q) = \frac{A\zeta^2}{2} + \frac{2\pi B}{q^2\zeta^2} \tag{3}$$

where *q* is the scattering vector parallel to the surfaces. *A* and *B* are constants, dependent on the surface tension of the liquid, i.e., the roughness. Figure 7 shows that the data do not fit the capillary wave theory over a broad *q* range, although a fit over a restricted range of wavevectors was possible. Examination of the data in log−log form (see Figure 8) indicates a q^{-3} scaling

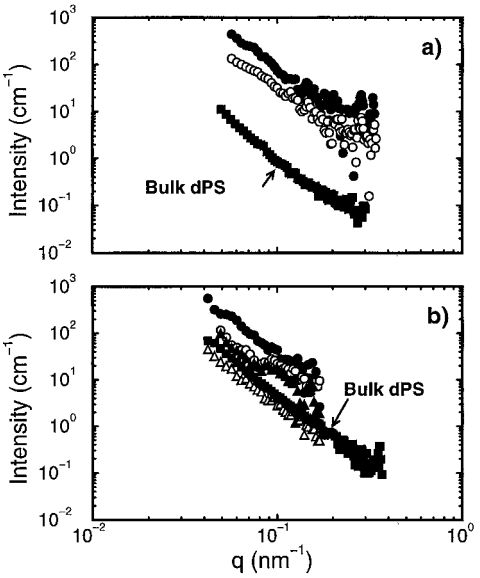

Figure 8. Logarithmic intensity vs logarithmic *q* for pure dPS films of molecular weight (a) 270K and (b) 650K. Displayed are thicknesses of (270K): 17 nm (solid circles), 60 nm (open circles), and bulk (solid squares); (650K): 15 nm (solid circles), 37 nm (open circles), 46 nm (closed triangles), 315 nm (open triangles), and bulk (solid squares).

instead of the predicted q^{-2} from theory. Since this scaling exponent is practically the same as that seen for the bulk, we have chosen to take the ratio of the thin film dPS scattering to its bulk analogue. We find that the ratio is independent of *q* and increases monotonically with decreasing thickness, confirming that all samples have the same q^{-3} scaling. At this time we have no explanation for this effect, except that we know that the thin film scattering, which appears to depend on the area of the film and not on its volume, is driven by the surfaces of the film. We have therefore empirically modeled the scattering of the thin dPS films by the form

$$I_{\text{surface}}(q) = \frac{I(q=0)}{q^3\xi^3_{\text{surface}}} \tag{4}$$

where ξ_{surface} is a correlation length. Note that in this form the relevant quantity is the ratio $I(q=0)/\xi^3_{\text{surface}}$, which is the single fit parameter for the dPS data. This has been utilized to analyze all blend data reported here. In past work we had modeled the thin film dPS scattering using a Debye−Bueche form.[27] While quantitatively different from past work, we shall show below that this change in analysis does not alter our primary conclusions regarding chain conformations and system thermodynamics in these thin films.

3.2.2. Blend Films. Blend scattering data for a range of film thicknesses for both molecular weights are presented in Figure 9. While nearly 20 different sets of films were measured during the course of these experiments, only three representative data sets from each molecular weight (270K and 650K) will be discussed. The total scattering intensity, $I(q)$, was fit to the functional form

$$I(q) = I_{\text{surface}}(q) + I_{\text{RPA}}(q) + I_{\text{incoherent}} \tag{5}$$

where the first term corresponds to the surface scattering (following eq 4) and the last term is a constant incoherent scattering (0.38 cm^{-1}). The second term,

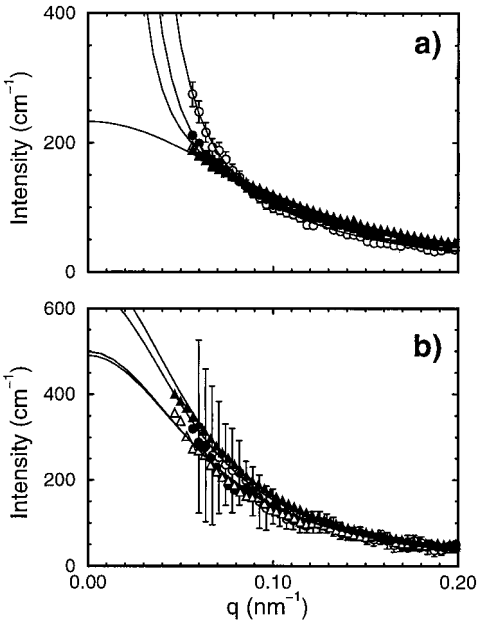

Figure 9. Intensity vs q plot for thin film blends of (a)270K dPS/hPS and (b) 650K dPS/hPS. Film thicknesses shown are (a) 60 nm (open triangles), 30 nm (solid circles), and 18 nm (open circles); (b) 150 nm (open triangles), 40 nm (solid circles), and 14 nm (open circles). For both molecular weights, an analogous bulk is included for comparison (solid triangles). Solid lines indicate a fit using the theoretical model described in the text.

arising from concentration fluctuations in the system, is described by the incompressible random phase approximation (RPA),[34]

$$\frac{k_N}{I_{RPA}(q)} = \frac{1}{\phi_1 v_1 N_1 P_D(qR_G)} + \frac{1}{\phi_2 v_2 N_2 P_D(qR_G)} - 2\frac{\chi}{v_0} \quad (6)$$

ϕ_i, v_i, and N_i are respectively the volume fraction, molar volume, and the degree of polymerization of component i. χ is the Flory−Huggins interaction parameter. P_D is the Debye single chain form factor, which is a function of the radius of gyration R_G:

$$P_D(qR_G) = \frac{2}{(q^2R_G^2)^2}[\exp(-q^2R_G^2) - 1 + q^2R_G^2] \quad (7)$$

For thick films (D > 60 nm), the total scattering intensity is equal to the bulk value within experimental uncertainties. In the 650K blend, this correspondence with bulk scattering extends down to $D < R_{G,bulk}$. For the 270K blend, however, the scattering at low-q vectors increases by a factor of 1.5 in the thinner films (17 nm < D < 60 nm). Given the inherent doubling of the coherent scattered intensity in the 650K vs 270K blends due to molecular weight (eq 6), it is reasonable that the surface scattering contribution is less important than the concentration fluctuation term for the high molecular weight blends at low q.

By varying χ, the segment length, σ, and $I_{surface}(0)/\xi^3_{surface}$, we obtained a fit to each set of experimental data sets. An example of the relative contributions of each component to the total fit is shown in Figure 10. It is clear that the q^{-3} dependence of the roughness term is prominent at low q, while the q^{-2} dependence of the RPA contributes out to significantly higher q. While this separation of length scales allows independent fitting

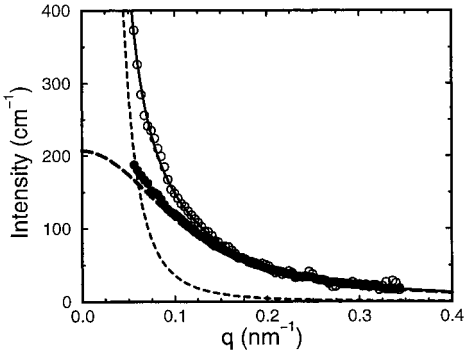

Figure 10. Intensity plotted as a function of q for a thin film blend of thickness 17 nm (open circles). In addition, results from a bulk sample are presented (filled circles). The components of the fit of the thin film data to eq 5 are shown: standard RPA (long dashed line), surface term (short dashed line), and sum of both contributions (solid line).

Table 2. Fit Parameters to Low-q Data for the 270K Blend[a]

	RPA only				RPA + roughness			
D (nm)	σ (nm)	χ ($\times 10^6$)	$S(0)$ (cm^{-1})	ξ (nm)	σ (nm)	χ ($\times 10^6$)	$S(0)$ (cm^{-1})	ξ (nm)
15	0.77	4.8	400	13	0.73	−1.4	180	9
17	0.92	6.1	540	19	0.85	−4.4	150	9
18	0.79	7.4	820	20	0.68	−0.1	210	9
31	0.64	6.3	570	13	0.67	3.5	320	10
32	0.69	4.8	400	12	0.64	1.6	250	9
34	0.80	2.7	290	12	0.74	−1.7	180	9
40	0.68	2.3	270	9.8	0.62	1.8	260	9
41	0.80	2.9	300	12	0.68	1.9	260	10
41	0.63	3.2	300	9.5	0.74	−3.7	150	8
43	0.67	3.0	300	10	0.71	2.9	300	11
59	0.72	0.7	220	9.4	0.72	−0.3	200	9
60	0.54	−1.4	180	6.4	0.67	−0.3	200	8
61	0.69	1.1	230	9.2	0.69	−0.3	200	9
61	0.77	5.1	420	14	0.67	−1.1	190	8
62	0.80	2.2	270	11	0.71	−2.5	170	8
62	0.73	2.2	270	11	0.70	−0.6	200	9
85	0.68	5.3	450	12	0.69	3.3	310	11
175	0.64	0.9	230	8.5	0.68	3.4	320	11

[a] Results from a pure RPA fit and a combination of RPA and roughness terms are shown.

of the two terms, the fits here were performed simultaneously to prevent bias. The results of all fits are summarized in Tables 2 and 3 and in Figure 11.

In agreement with our past results,[27,29] and also with the Kratky results discussed above, the statistical segment length (and hence the radius of gyration parallel to the surfaces) is identical to its bulk value for all films considered. Note that the film thickness varies over 2 orders of magnitude in these studies. The data have been fit both with and without the correction for surface scattering (eq 4), with fit values of the segmental length being essentially independent of the analysis procedure (Table 2).

This is in contrast to the χ parameters, which are quite sensitive to the inclusion of the surface term (Tables 2 and 3). However, the extremely small magnitude of χ results in large uncertainties. Error bars for the 270K blend demonstrate an uncertainty which is on average an order of magnitude larger than the χ values obtained. (The errors for the 650K data are not shown for clarity.) To within these large uncertainties we find a lack of finite size effects on system thermodynamics. However, this result is not surprising since the annealing temperature is more than 125° C above the bulk spinodal even for the 650K blend.

Table 3. Fit Parameters to Low-*q* Data for the 650K Blend[a]

D (nm)	σ (nm)	χ ($\times 10^7$)	$S(0)$ (cm^{-1})	ξ (nm)
14	0.73	0.06	650	16
14	0.70	−0.82	170	8
30	0.68	−0.23	340	11
30	0.78	0.04	600	17
33	0.67	−0.23	340	11
37	0.75	−0.03	500	15
62	0.74	−0.06	460	14
62	0.65	−0.64	200	8
73	0.66	0.02	570	14
99	0.74	−0.10	430	14
99	0.65	0.09	700	15
116	0.73	0.03	580	15
156	0.72	0.02	530	15
156	0.73	0.05	630	16
237	0.70	−0.03	500	14
450	0.74	0.06	640	16
480	0.63	−0.32	290	9
838	0.72	0.00	530	15
939	0.72	0.02	570	15

[a] Results from a pure RPA fit.

3.2.3. Role of Surface Segregation on Scattering. We have utilized the mean-field theory of Flebbe et al.[35] to obtain the surface segregation of dPS to the two surfaces. The parameters corresponding to the 270K blend were used in this calculation (see Appendix). In Figure 12, calculated composition profiles are provided for a range of film thicknesses ($0.5 < D/R_{G,bulk} < 7.5$). As found previously,[36] the composition profile flattens when the film thickness is of the order $R_{G,bulk}$.

We now use this information to predict the zero wavevector limit of the scattering from these thin film blends. The scattering intensity at zero wave vector is obtained through the definition

$$S(q=0)^{-1} = \frac{\delta^2 F_{mix}}{\delta \bar{\phi}^2} \tag{8}$$

where F_{mix} is an appropriate free energy and $\bar{\phi}$ is the average composition of the film.

Since the scattering vector in our experiments is in the plane of the film, we are insensitive to variations in the z direction. In this calculation, we ignore all terms in the free energy functional related to gradients and the surface potential (see Appendix), and therefore, we consider only the Flory−Huggins free energy of mixing contributions integrated over the concentration profile. The predicted scattering is identical to the bulk and thus in agreement with experiment. In contrast, if one could conduct an experiment where the scattering vector were in the z direction, then the whole free energy functional would be utilized in this prediction. The suppression of the profile results in a greatly decreased total scattered intensity (see Figure 13).

4. Discussion

It is well established that the density of films as thin as $D/R_{G,bulk} = 0.5$ are essentially the same as the bulk value.[37,38] Brown and Russell[39] suggest that the constraints of bulklike density and an essentially Gaussian conformation parallel to the surface imply that these chains have lowered intermolecular entanglement in films thinner than $R_{G,bulk}$. This is easy to see by computing the intramolecular density inside a coil: $\rho_{intra} = N R_{G,xy}^{-2} R_{G,z}^{-1}$. Since $R_{G,xy}$ effectively assumes its bulk value, but $R_{G,z}$ is strongly reduced, we can see that ρ_{intra} $\gg \rho_{bulk}$. These results are further supported by prior studies of polystyrene chains cast on liquid substrates.[40−42] There, aggregation of the molecules led to bulk densities. While the degree of entanglement could not be directly measured, the solution properties, being in the very dilute regime, indicate that the entanglement in these molecules is low. This implies that confinement will have dramatic consequences on the dynamics and mechanical properties of thin films relative to their bulk counterparts. Such conclusions, indeed, appear to be in reasonable qualitative agreement with the diffusion and glass transition phenomena in thin films. However, this area is still in its nascent stage, and the connection between chain structure and properties is not fully understood at this time.

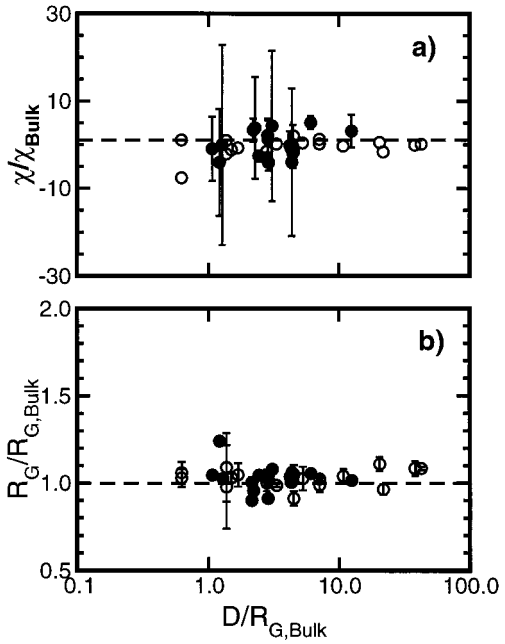

Figure 11. Effects of the film thickness on (a) the χ parameter and (b) R_G. Note that the x-axis is normalized by $R_{G,bulk}$ and that the χ and R_G values are normalized to their bulk counterparts, so as to correct for instrument variations during the 2 year span over which these data were taken. Data are reported for both 270K (solid circles) and 650K (open circles) blends. Data were analyzed by standard RPA analysis after subtraction of interfacial roughness scattering.

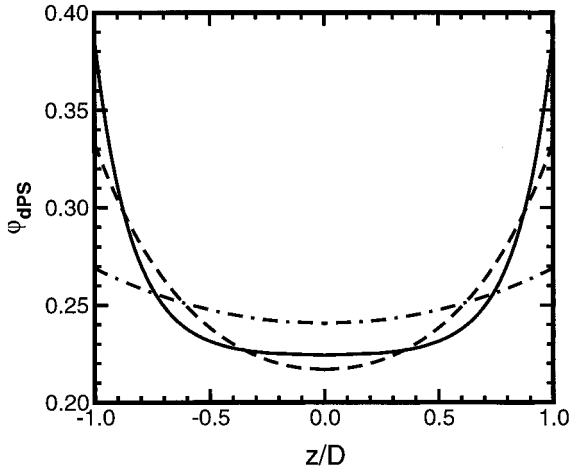

Figure 12. Volume fraction of dPS, ϕ_{dPS}, as a function of the distance from the center of the film, z, as obtained from mean-field theory outlined in the text. Data represent predictions for films of total thickness 10 (dot dashed line), 50 (dashed line), and 150 (solid line) lattice units.

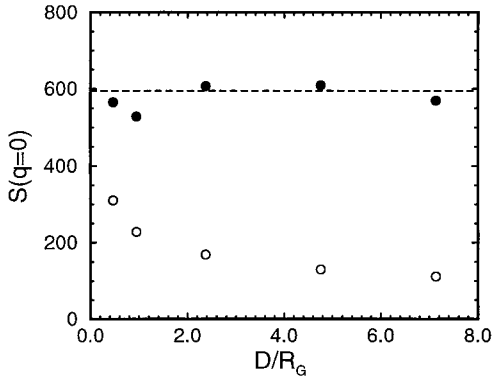

Figure 13. Predicted zero angle structure factor, $S(q=0)$, as a function of the reduced overall film thickness D/R_G, where R_G is the radius of gyration. Shown are data for the total scattered intensity (open circles) and the intensity resulting only from terms parallel to the substrate (solid circles). The analogous bulk result is also given (dashed line). Results are obtained from mean-field theory outlined in the text.

5. Conclusions

We have utilized SANS to probe the molecular conformation of polystyrene chains in ultrathin films where the total thickness ranges from bulk to sub $R_{G,bulk}$. An RPA analysis and a Kratky analysis independently and unequivocally verify that chains retain their Gaussian coil shape parallel to the surfaces with an apparently unperturbed statistical segment length for all of the films considered. In all of these cases we have found that it is crucial to properly account for parasitic scattering that arises mainly from the roughness of the air and substrate interfaces of the film. Our conclusions for chain conformations in thin films are in agreement with the many simulations conducted for polymer melts in confined geometries, all of which suggest that chain dimensions normal to the confinement direction are affected little, even if the films thicknesses are comparable to the unperturbed radius of gyration of the chains. These results are expected to strongly affect the dynamics of chains, an area of focus in our research groups.

Acknowledgment. We thank C. Glinka for helpful discussions concerning neutron scattering. Funding for S.K. and R.J. was provided by the National Science Foundation, Division of Materials Research (DMR-9804327), and the American Chemical Society, Petroleum Research Fund. We acknowledge the support of the National Institutes of Standards and Technology, U.S. Department of Commerce, in providing facilities used in this work. This material is based upon activities supported by the National Science Foundation under Agreement DMR-9986442.

Appendix: Effects of Surface Segregation

Surface segregation in polymer blend thin films has been extensively measured in isotopic polystyrene.[43,44] For these molecular weights and composition, the deuterated component preferentially segregates to both the silicon and the vacuum surface.[44] To delineate this surface segregation, we write the free energy functional in a Landau−Ginzburg form

$$\frac{F_{mix}}{k_B T} \equiv \frac{F_{blend} + F_{surf}}{k_B T} \equiv \int_0^{D/2} d\phi \, [f_{mix}(\phi) + \kappa(\nabla\phi)^2] - \mu_1\phi_1 - g_1{\phi_1}^2 - \mu_2\phi_2 - g_2{\phi_2}^2 \quad (9)$$

where f is the Flory free energy of mixing. The second term in the integral represents the penalty for forming a gradient, and the prefactor κ has the mean-field form[34] [$= a^2/(36\phi(1-\phi))$ where a is the Kuhn segment length]. For this study, parameters were chosen to mimic the 270K blend at 120° C, namely $N = 2700$, $a = 0.68$ nm, and $\chi = 1.0 \times 10^{-4}$. The terms outside of the integral are due to the surfaces, labeled as 1 and 2, where μ is the excess chemical potential of the surface, and g represents the penalty for the "loss of nearest neighbors" effect. Using standard techniques, this functional can be minimized and solved for the equilibrium composition profile. The second derivative of the total free energy is then directly related to the inverse scattered intensity as

$$\frac{k_N \nu_0}{I(q=0)} = \frac{\partial^2 (F_{mix}/k_B T)}{\partial \phi^2} \quad (10)$$

Numerical integration provided the free energy for a series of compositions from 24.5 to 25.5 wt % dPS. Integration was performed using an integration step of $d\phi = 1 \times 10^{-7}$. Even at this small value, the error involved in the final free energy produced large errors in the numerical estimate of scattering intensity. Further decreases in the integration step were not possible due to propagation of errors which exceeded double-precision limits. Therefore, a series of free energies were calculated over a range of compositions and subsequently fit using a quadratic polynomial. The second derivative was then analytically extracted. Assuming the surface potentials to be symmetric, and following the methods of Flebbe et al.,[35] the free energy was evaluated using published surface potentials ($\mu_1 = 0.001$, $g_1 = -0.0007$).[43]

Note Added After ASAP Posting

This article was released ASAP on 1/6/2001 with minor errors in eqs 1, 2, and 4. The correct version was posted 1/09/2001.

References and Notes

(1) Yethiraj, A.; Hall, C. *J. Chem. Phys.* **1991**, *95*, 1999.
(2) Bitsanis, I.; ten Brinke, G. *J. Chem. Phys.* **1993**, *99*, 3100.
(3) Kumar, S.; Vacatello, M.; Yoon, D. *J. Chem. Phys.* **1988**, *89*, 5206.
(4) Pakula, T. *J. Chem. Phys.* **1991**, *95*, 4685.
(5) Mansfield, K.; Theodorou, D. *Macromolecules* **1991**, *24*, 6283.
(6) Silverberg, A. *J. Colloid Interface Sci.* **1982**, *90*, 86.
(7) Weber, M. F.; Stover, C. A.; Gilbert, L. R.; Nevitt, T. J.; Ouderkirk, A. J. *Science* **2000**, *287*, 2451.
(8) Factor, B.; Russell, T.; Toney, M. *Phys. Rev. Lett.* **1991**, *66*, 1181.
(9) Zheng, X.; Rafailovich, M.; Sokolov, J.; Strzhemechny, Y.; Schwarz, S.; Sauer, B.; Rubenstein, M. *Phys. Rev. Lett.* **1997**, *79*, 241.
(10) Keddie, J.; Jones, R. A. L.; Cory, R. *Europhys. Lett.* **1994**, *27*, 59.
(11) Keddie, J.; Jones, R. A. L.; Cory, R. *Faraday Discuss.* **1994**, *98*, 219.
(12) Wallace, W.; van Zanten, J.; Wu, W. *Phys. Rev. E* **1995**, *52*, R3329.
(13) van Zanten, J.; Wallace, W.; Wu, W. *Phys. Rev. E* **1996**, *53*, R2053.
(14) Dalnoki-Veress, J. F. K.; Stevens, J.; Dutcher, J. *Phys. Rev. Lett.* **1996**, *77*, 2002.
(15) Zhao, W.; Rafailovich, M.; Sokolov, J.; Fetters, L.; Plano, R.; Sanyal, M.; Sinha, S.; Sauer, B. *Phys. Rev. Lett.* **1993**, *70*, 1453.
(16) Wiltzius, P.; Dierker, S.; Dennis, B. *Phys. Rev. Lett.* **1989**, *62*, 804.
(17) Frisken, B.; Cannell, D. *Phys. Rev. Lett.* **1992**, *69*, 632.

(18) Lin, M.; Sinha, S. K.; Drake, J.; Wu, X.; Thiyagarajan, P.; Stanley, H. *Phys. Rev. Lett.* **1994**, *72*, 2207.
(19) Frisken, B.; Cannell, D.; Lin, M.; Sinha, S. *Phys. Rev. E* **1995**, *51*, 5866.
(20) Dierker, S.; Wiltzius, P. *Phys. Rev. Lett.* **1991**, *66*, 1185.
(21) Lal, J.; Sinha, S. K.; Auvray, L. *J. Phys. (Paris)* **1997**, *10*, 1597.
(22) Shuto, K.; Oishi, Y.; Kajiyama, T.; Han, C. C. *Polym. J.* **1993**, *25*, 291.
(23) Shuto, K.; Oishi, Y.; Kajiyama, T.; Han, C. C. *Macromolecules* **1993**, *26*, 6589.
(24) Kraus, J.; Mueller-Buschbaum, P.; Kuhlman, T.; Schubert, D.; Stamm, M. *Europhys. Lett.* **2000**, *49*, 210.
(25) Shuto, K.; Oishi, Y.; Kajiyama, T. *Polymer* **1995**, *36*, 549.
(26) Brulet, A.; Boue, F.; Menelle, A.; Cotton, J. *Macromolecules* **2000**, *33*, 997.
(27) Jones, R. L.; Kumar, S. K.; Ho, D.; Briber, R. M.; Russell, T. P. *Nature* **1999**, *400*, 146.
(28) Lambooy, P.; Barker, J. G.; Gallagher, P. D.; Satija, S. K.; Kellogg, G. J.; Mayes, A. M.; Russell, T. P. *Macromolecules* **1995**, *28*, 787.
(29) Ho, D.; Briber, R. M.; Jones, R. L.; Kumar, S. K.; Russell, T. P. *Macromolecules* **1998**, *26*, 9247.
(30) Londono, J.; Narten, A.; Wignall, G.; Honnell, K. G.; Hsieh, E.; Johnson, T.; Bates, F. *Macromolecules* **1994**, *27*, 2864.
(31) Xie, R.; Karim, A.; Douglas, J. F.; Han, C. C.; Weiss, R. A. *Phys. Rev. Lett.* **1998**, *81*, 1251.
(32) Balsara, N.; Lohse, D.; Graessley, W.; Krishnamoorti, R. *J. Chem. Phys.* **1994**, *100*, 3905.
(33) Sinha, S. *J. Phys. C* **1985**, *18*, 6427.
(34) deGennes, P. *Scaling Concepts in Polymer Physics*; Cornell University Press: Ithaca, NY, 1979.
(35) Flebbe, T.; Dunweg, B.; Binder, K. *J. Phys. II* **1996**, *6*, 667.
(36) Hariharan, A.; Kumar, S. K.; Russell, T. P. *J. Chem. Phys.* **1993**, *99*, 4041.
(37) Wallace, W.; Tan, N. B.; Wu, W. L.; Satija, S. *J. Chem. Phys.* **1998**, *108*, 3798.
(38) Wallace, W.; Tan, N. B.; Wu, W. L.; Satija, S. *J. Chem. Phys.* **1998**, *108*, 3798.
(39) Brown, H.; Russell, T. P. *Macromolecules* **1996**, *29*, 798.
(40) Kumaki, J. *Macromolecules* **1988**, *21*, 749.
(41) Kawaguchi, M.; Yoshida, A.; Takahashi, A. *Macromolecules* **1983**, *16*, 956.
(42) Vilanove, R.; Rondelez, F. *Phys. Rev. Lett.* **1980**, *45*, 1502.
(43) Jones, R. A. L.; Kramer, E. J.; Rafailovich, M.; Sokolov, J.; Schwarz, S. *Phys. Rev. Lett.* **1989**, *62*, 280.
(44) Jones, R. A. L.; Norton, L.; Kramer, E. J.; Composto, R.; Stein, R.; Russell, T.; Mansour, A.; Karim, A.; Felcher, G.; Rafailovich, M.; Sokolov, J.; Zhao, X.; Schwarz, S. *Europhys. Lett.* **1990**, *12*, 41.

MA001141O